

# Modeling hybrid stars with an SU(3) nonlinear $\sigma$ model

Rodrigo Nereiros\*

Frankfurt Institute for Advanced Studies, Goethe University, Ruth Moufang Strasse 1, D-60438 Frankfurt am Main, Germany

V. A. Dexheimer†

Gettysburg College, Gettysburg, Pennsylvania, 17325 USA

S. Schramm‡

Center for Scientific Computing, Frankfurt Institute for Advanced Studies, Institut für Theoretische Physik, Johann Wolfgang Goethe University, D-60438 Frankfurt am Main, Germany

(Received 28 May 2010; revised manuscript received 11 July 2010; published 21 September 2010)

We study the behavior of hybrid stars by using an extended hadronic and quark SU(3) nonlinear sigma model. The degrees of freedom change naturally, in this model, from hadrons to quarks as the density/temperature increases. At zero temperature, we reproduce massive neutron stars, which contain cores of hybrid matter of 2 km for the nonrotating case and 1.18 and 0.87 km, in the equatorial and polar directions, respectively, for stars that rotate at the Kepler frequency (physical cases lie in between). The cooling of such stars is also analyzed.

DOI: [10.1103/PhysRevC.82.035803](https://doi.org/10.1103/PhysRevC.82.035803)

PACS number(s): 26.60.Dd, 11.30.Rd, 21.65.Qr, 97.60.Jd

## I. INTRODUCTION

As the densest bodies in the universe, neutron stars are one of the best-suited candidates in which to look for quark matter. The study of when and how the deconfinement from hadronic to quark matter occurs is crucial for the understanding and identification of such phenomena. Usual approaches for hybrid neutron stars consist of two different models with separate equations of state for hadronic and quark phases (see, e.g., Ref. [1]), connected at the point for which the pressure of the quark phase exceeds that of the hadronic one. Within our approach, we employ a single model for the hadronic and quark phases, which avoids the need for two separate equations of state. This approach, which presents a more natural transition from hadronic to quark matter, allows us to follow the spin evolution of a hybrid star with a single equation of state. In this paper, we will investigate the structural changes that follow the stellar spin down and the subsequent effects on the cooling of the object.

The SU(3) nonlinear  $\sigma$  model introduces baryons and quarks as flavor-SU(3) multiplets. Baryons and quarks obtain their masses through their coupling to the scalar fields of the theory (with an additional coupling to the Polyakov loop as discussed in the following) via spontaneous symmetry breaking. We include the quark degrees of freedom in the hadronic model in analogy to the Polyakov-loop extended Nambu-Jona-Lasinio (PNJL) model [2] by using an effective field that can be related to the QCD Polyakov loop, defined via  $\Phi = \frac{1}{3} \text{Tr} [\exp(i \int d\tau A_4)]$ , where  $A_4 = iA_0$  is the temporal component of the SU(3) gauge field. The effect of the field is to suppress quarks in the low-density/temperature regime and baryons at high densities and temperatures, respectively.

This paper is divided as follows: in Sec. II, we review the properties of the model used for the composition and equation of state; in Sec. III, we present our results, which encompass the structure of rotating and spherically symmetric compact stars and cooling effects; and in Sec. IV, our conclusions are presented.

## II. THE MODEL

The Lagrangian density for the  $\sigma$ -type model, in mean-field approximation, is given by

$$L = L_{\text{Kin}} + L_{\text{Int}} + L_{\text{Self}} + L_{\text{SB}} - U, \quad (1)$$

where, in addition to the kinetic-energy term for hadrons, quarks, and leptons, the terms,

$$L_{\text{Int}} = - \sum_i \bar{\psi}_i [\gamma_0 (g_{i\omega} \omega + g_{i\phi} \phi + g_{i\rho} \tau_3 \rho) + M_i^*] \psi_i, \quad (2)$$

$$\begin{aligned} L_{\text{Self}} = & -\frac{1}{2} (m_\omega^2 \omega^2 + m_\rho^2 \rho^2 + m_\phi^2 \phi^2) \\ & + g_4 \left( \omega^4 + \frac{\phi^4}{4} + 3\omega^2 \phi^2 + \frac{4\omega^3 \phi}{\sqrt{2}} + \frac{2\omega \phi^3}{\sqrt{2}} \right) \\ & + k_0 (\sigma^2 + \zeta^2 + \delta^2) + k_1 (\sigma^2 + \zeta^2 + \delta^2)^2 \\ & + k_2 \left( \frac{\sigma^4}{2} + \frac{\delta^4}{2} + 3\sigma^2 \delta^2 + \zeta^4 \right) + k_3 (\sigma^2 - \delta^2) \zeta \\ & + k_4 \ln \frac{(\sigma^2 - \delta^2) \zeta}{\sigma_0^2 \zeta_0}, \end{aligned} \quad (3)$$

$$L_{\text{SB}} = m_\pi^2 f_\pi \sigma + \left( \sqrt{2} m_k^2 f_k - \frac{1}{\sqrt{2}} m_\pi^2 f_\pi \right) \zeta \quad (4)$$

represent the baryon (and quark) meson interactions, meson self-interactions, and an explicit chiral symmetry-breaking term that is responsible for producing the masses of the pseudoscalar mesons. We will discuss the potential  $U$  further along in this paper. The model has an SU(3)-flavor symmetry,

\*nereiros@fias.uni-frankfurt.de

†vantoche@gettysburg.edu

‡schramm@th.physik.uni-frankfurt.de

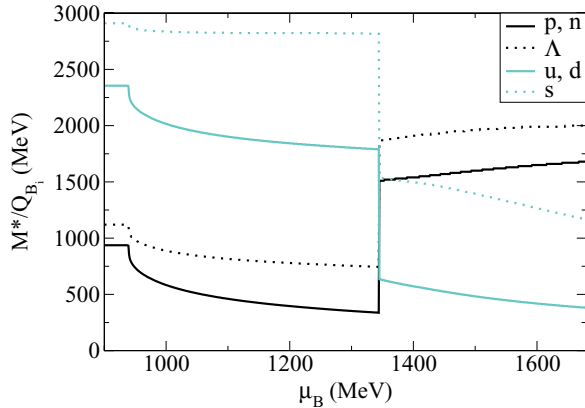


FIG. 1. (Color online) Effective normalized mass of different species as a function of baryonic chemical potential for star matter at zero temperature [3].

and the index  $i$  denotes the baryon octet and the three light quarks. In our calculations, we take the following mesons: the vector isoscalars  $\omega$  and  $\phi$ , the vector isovector  $\rho$ , the scalar isoscalars  $\sigma$  and  $\zeta$  (nonstrange and strange quark-antiquark states, respectively), and the scalar isovector  $\delta$  into account. The coupling constants of the model can be found in Ref. [3]. They were fitted to reproduce the vacuum masses of the baryons and mesons, nuclear saturation properties (density  $\rho_0 = 0.15 \text{ fm}^{-3}$ , binding energy per nucleon  $B/A = -16.00 \text{ MeV}$ , nucleon effective mass  $M_N^* = 0.67 M_N$ , and compressibility  $K = 297.32 \text{ MeV}$ ), asymmetry energy ( $E_{\text{sym}} = 32.50 \text{ MeV}$ ), and reasonable values for the hyperon potentials ( $U_\Lambda = -28.00 \text{ MeV}$ ,  $U_\Sigma = 5.35 \text{ MeV}$ , and  $U_\Xi = -18.36 \text{ MeV}$ ). The vacuum expectation values of the scalar mesons are constrained by reproducing the pion- and kaon-decay constants. A detailed discussion of

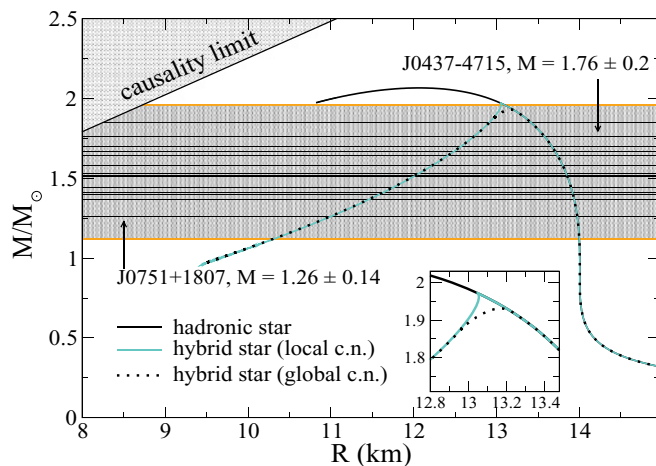


FIG. 2. (Color online) Mass-radius diagram for the model investigated in this paper. The horizontal lines represent observed pulsar masses (Refs. [11–17] and references therein). The band delimited by the two thick horizontal lines (orange) represent the range of pulsar masses observed, which account for the error of the highest and lowest observed masses. c.n., charge neutrality.

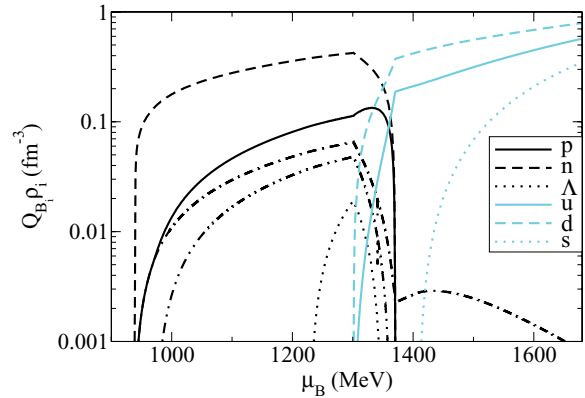


FIG. 3. (Color online) Population (baryonic density for different species as a function of baryonic chemical potential) for star matter at zero temperature by using global c.n. [3].

the purely hadronic part of the Lagrangian can be found in Refs. [4–6].

The effective masses of the baryons and quarks are given by

$$M_B^* = g_{B\sigma}\sigma + g_{B\delta}\tau_3\delta + g_{B\zeta}\zeta + M_{0_B} + g_{B\Phi}\Phi^2, \quad (5)$$

$$M_q^* = g_{q\sigma}\sigma + g_{q\delta}\tau_3\delta + g_{q\zeta}\zeta + M_{0_q} + g_{q\Phi}(1 - \Phi), \quad (6)$$

where  $M_0$  is equal to 150 MeV for nucleons, 354 MeV for hyperons, 5 MeV for up and down quarks, and 150 MeV for strange quarks.

Equations (5) and (6) show that, as the field  $\Phi$  increases (with the increase in density/temperature), baryons are suppressed, which gives way to the quark phase, effectively to model the QCD deconfinement phase transition. The opposite is true for low values of  $\Phi$  (at low density/temperature).

The effective normalized masses of baryons and quarks are shown in Fig. 1. Since the coupling constants in the  $\Phi$  term of the effective mass formulas are high but still finite, the effective masses of the species not present in each phase are large but also finite.

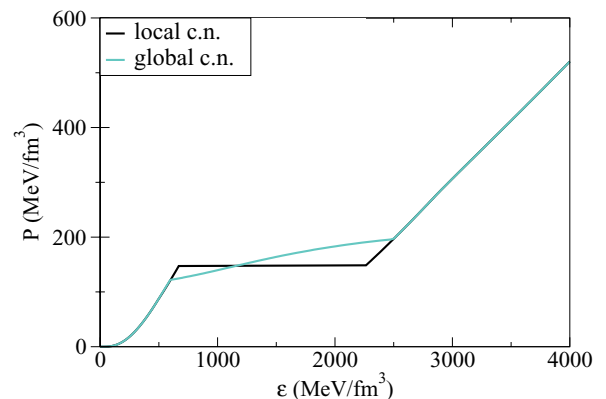


FIG. 4. (Color online) Equation of state (pressure as a function of energy density) for star matter at zero temperature by using local and global c.n. [3].

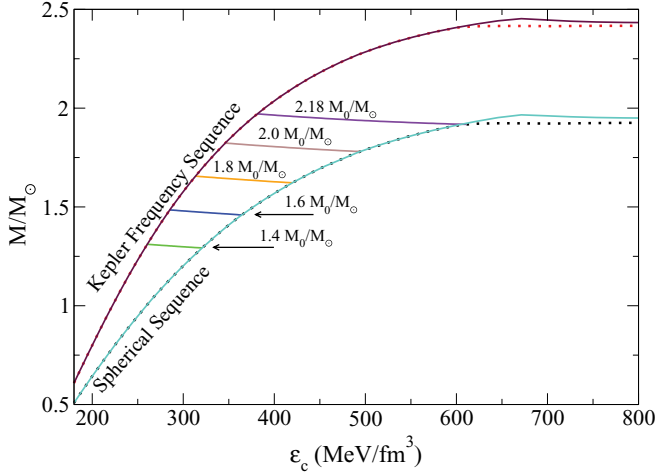


FIG. 5. (Color online) Gravitational mass as a function of central density. The lowermost sequences represent static stars ( $\Omega = 0$  Hz), whereas the highermost sequence represents stars that rotate at their Kepler frequency. The curves that connect the Kepler frequency to the static sequence are for stars with constant baryonic mass. These sequences represent the evolution of Kepler frequency stars to nonrotating objects.

In analogy to the PNJL model, we define the potential  $U$  for  $\Phi$  as

$$U = (a_0 T^4 + a_1 \mu^4 + a_2 T^2 \mu^2) \Phi^2 + a_3 T_0^4 \log(1 - 6\Phi^2 + 8\Phi^3 - 3\Phi^4). \quad (7)$$

In our case,  $U(\Phi)$  is a simplified version of the potential used in Refs. [7,8] and adapted to include terms that depend on the chemical potential. These two extra terms are not unique but are the most simple natural choice for extending the potential. The corresponding parameters are chosen to reproduce the main features of the phase diagram at finite densities. The coupling constants for the quarks can be found in Ref. [3] and are chosen to reproduce lattice data as well as known information about the phase diagram. The lattice data

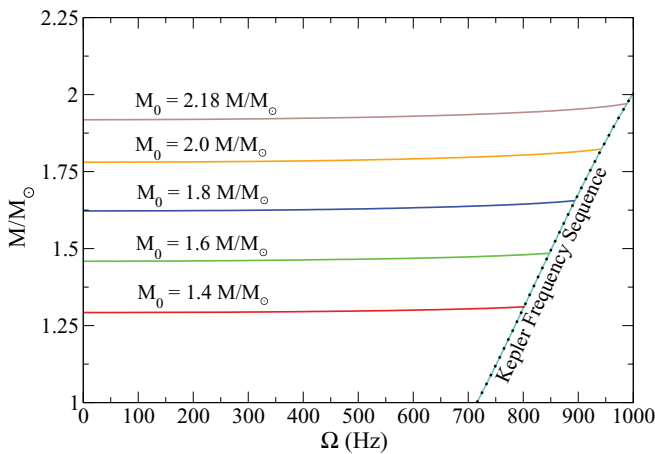


FIG. 6. (Color online) Gravitational mass as a function of frequency for the stars of Fig. 5. The stars from the static sequence are on the y axis of the graph.

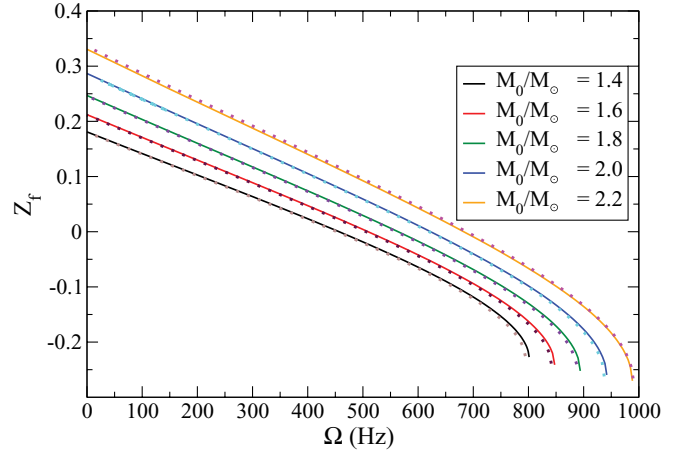


FIG. 7. (Color online) Forward redshift for the constant baryon mass sequences of Fig. 5. The dotted lines represent the redshift of the equivalent sequence for purely hadronic matter, which are almost identical to that of hybrid stars.

include a first-order phase transition at  $T = 270$  MeV and a pressure function  $P(T)$  similar to Refs. [7,8] at  $\mu = 0$  for pure gauge (for the quenched case without hadrons and quarks).

### III. RESULTS

#### A. Deconfinement to quark matter

In our model, the quarks are suppressed in the hadronic phase, and the hadrons are suppressed in the quark phase up to  $\mu_B = 1700$  MeV for  $T = 0$ . This behavior is caused by the fact that the coupling constants in the  $\Phi$  term of the effective mass formulas are high but still finite, so, in principle, at very high chemical potential, the threshold for hadrons can be reached a second time. This threshold, which is higher than the density in the center of the neutron stars, establishes a limit for the applicability of the model. The hyperons,

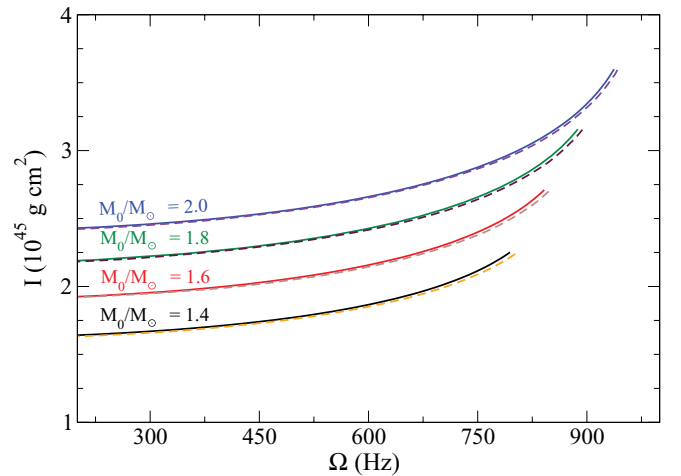


FIG. 8. (Color online) Moment of inertia for the constant baryon mass sequences of Fig. 5. During the spin down, the geometry of the objects changes significantly; and, therefore, the moment of inertia for these stars is substantially modified.

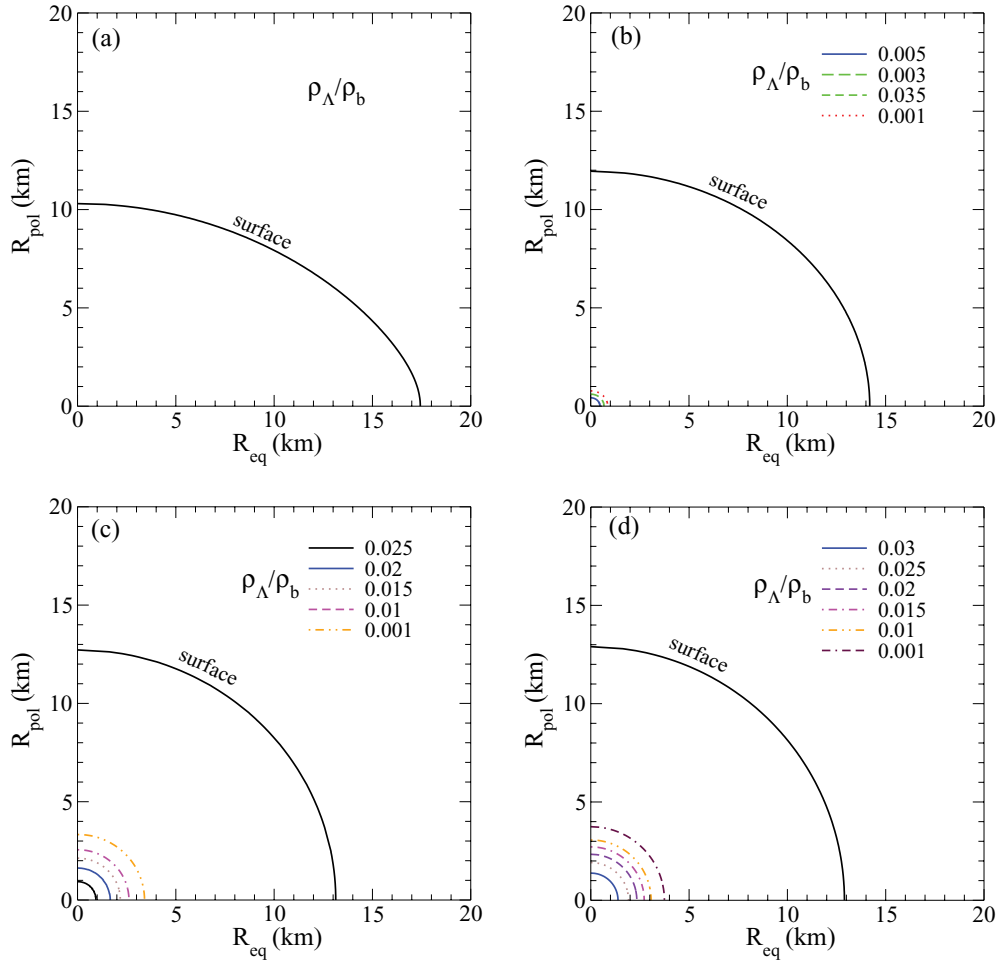


FIG. 9. (Color online) Strangeness content for a compact star with  $M_0/M_\odot = 2.18$  for frequencies of (a) 988.4 Hz, (b) 746.0 Hz, (c) 356.3 Hz, and (d) 0.0 Hz. The  $z$  axis represents the relative population of  $\Lambda$  ( $\rho_\Lambda/\rho_b$ ).

despite being included in the calculation, are suppressed by the appearance of the quark phase. Only a very small amount of  $\Lambda$ 's appears immediately before the phase transition. The strange quarks appear after the other quarks with relatively low abundance. The density of electrons and muons is significant in the hadronic phase but not in the quark phase, since the down and strange quarks are negatively charged, which reduces the need for leptons to maintain c.n.

By focusing on the high-density/low-temperature region of the phase diagram, we are able to calculate neutron star masses and radii, which are solutions of the Tolman-Oppenheimer-Volkoff equations [9,10]. The solutions for hadronic (same model but without quarks) and hybrid stars are shown in Fig. 2, where, in addition to our equation of state for the core, a separate equation of state was used for the crust [18]. The horizontal lines in Fig. 2 represent observed masses of some prominent millisecond pulsars (Refs. [11–17] and references therein). To avoid cluttering the graph, we only indicated the names of the pulsars that establish the lowest and highest observed masses: J0751 + 1807 with mass  $M/M_\odot = 1.26 \pm 0.14$  [15] and J0437 – 4715 with  $M/M_\odot = 1.76 \pm 0.2$  [11,14], respectively. Any plausible equation of state must be able to produce neutron stars within the range delimited by these two objects,

as is the case for the model investigated in this paper. Our model predicts a maximum neutron star mass of  $2.1 M_\odot$  by considering local charge neutrality, which, as shown in Fig. 2, is in agreement with the observational constraints shown. By comparing to the hadronic star sequence, the hybrid sequence has a much sharper peak. This peak (which denotes the most massive stable star in the sequence) signals the phase transition into quark matter at the core of the star. Because the equation of state for quark matter is much softer than the one for hadronic matter, the star becomes unstable at the point where the central density is higher than the phase-transition threshold.

There is still another possible option for the configuration of the particles in the neutron star [19]. If, instead of local, we consider global c.n., we find a mixture of phases even for zero temperature as discussed in Ref. [20]. This possibility, which is a more realistic approach, changes the particle densities in the coexistence region by making them appear and vanish in a smoother way (Fig. 3). Therefore, the maximum mass allowed for the star is slightly lower in this case than in the previous one, as can be seen from the dotted line in Fig. 2; however, this possibility allows stable hybrid stars with a small amount of quarks. The mixed phase constitutes the inner core of the

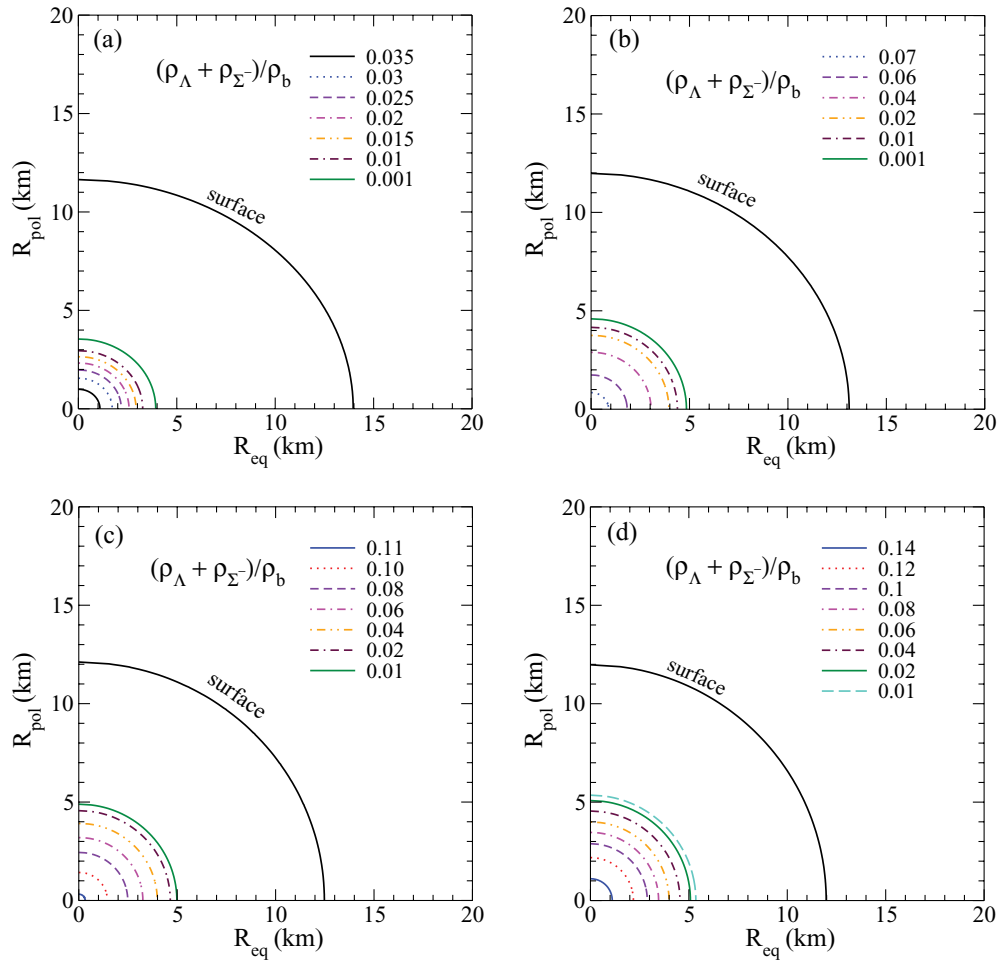


FIG. 10. (Color online) Strangeness content for a compact star with  $M_0/M_\odot = 2.38$  in the pure hadronic model. The frequencies are (a) 828.3 Hz, (b) 639.9 Hz, (c) 394.8 Hz, and (d) 0.0 Hz. The  $z$  axis represents the relative population of  $\Lambda$  and  $\Sigma^-$   $[(\rho_\Lambda + \rho_{\Sigma^-})/\rho_b]$ .

star up to a radius of approximately 2 km. The equation of state for both cases is shown in Fig. 4. The large jump in the pressure for the local c.n. case explains why the neutron stars become immediately unstable after the phase transition in this configuration.

### B. Rotational effects

The results shown in Fig. 2 are for static neutron stars without including rotational effects. The rotational nature of pulsars (which, in some cases, may be rotating with frequencies as high as 700 Hz) warrants the investigation of the structure of rapidly rotating neutron stars, which is considerably more complicated than that of static objects. In Refs. [6,21], the rotational effects of the hadronic part of our model were investigated by means of the improved Hartle-Thorne perturbative method [22]. Here, we will extend this research by performing exact rotational calculations and by including the quark phase described in Secs. II and III A. The numerical method used for the solution of Einstein's field equations, and for the stellar structure of rapidly rotating neutron stars is based on the Komatsu, Eriguchi, and Hachisu method [23], which basically consists of expanding the

metric functions in terms of Green's functions, which can be iteratively integrated, which allows us to calculate the structure of the star. This method has been expanded by several authors, and details can be found in Refs. [24,25].

In Fig. 5, we show the mass as a function of central density. The lowermost sequence represents static stars ( $\Omega = 0$  Hz), whereas the highest one represents stars that rotate at their Kepler frequencies. The Kepler frequency, or mass shedding frequency, is the maximum frequency at which a compact star may rotate. When rotating above this frequency, an object would shed mass at its equator. Therefore, this quantity sets an absolute limit for the frequency of compact stars. The curves that connect the Kepler frequency to the static sequence indicate stars with constant baryonic mass. These sequences represent the evolution of Kepler frequency stars to nonrotating objects. This is better illustrated in Fig. 6, which shows the gravitational mass as a function of frequency for the constant baryon mass stars. Figure 6 also shows that the gravitational mass may be as high as 3% higher for a star that rotates at the Kepler frequency (compared to a nonrotating star with the same baryonic mass). The central density, on the other hand, may be decreased by as much as 38%, as shown in Fig. 5. It is important to stress that the constant baryon mass sequences

shown in Figs. 5 and 6 represent the spin-down evolution of an isolated compact star (i.e., no accretion, hence, the constant baryon mass). Obviously, the spin-down evolution is a function of time; therefore, the  $x$  axis of Fig. 6 could just as well be replaced by time. How the frequency (or, equivalently, the central density) varies with time will depend on the spin-down rate of the star. The computation of this quantity is not trivial and depends on properties, such as magnetic field and/or gravitational radiation emission. Those issues are beyond the scope of the current paper; and, therefore, we show our results as a function of frequency and central density by always keeping the implicit time dependence in mind.

As shown in Figs. 5 and 6, when rotating at their Kepler frequencies, neutron stars can attain higher masses. Loosely speaking, this may be explained by the centrifugal force that provides an extra support against gravitational collapse. Although we can find stable rotating neutron stars with masses up to  $\sim 2.5$  solar masses, these objects will collapse into black holes during spin-down evolution, which might be observed by the sudden stop of the neutrino signal that originates from the star. As shown in Fig. 5, there is no stable static neutron star with a baryon mass greater than 2.18 solar masses predicted by our model.

The rotation also alters the redshift of the stars significantly. In Fig. 7, we show the forward redshift as a function of frequency for the stars of constant baryon mass from Fig. 5. As one can see, the forward redshift is substantially modified as the star's rotational frequency is reduced. In the extreme case of high frequencies, the forward redshift becomes negative. For comparison purposes, we also have plotted the redshift of the equivalent stellar sequences with no quark phase (purely hadronic matter). The redshift of these objects is almost identical to those of hybrid stars, with a very slight deviation for very high frequencies.

Just as the redshift is changed during the spin-down evolution, the moment of inertia of the star should be modified as well. The moment of inertia, as a function of frequency for the stars shown in Fig. 5, is given in Fig. 8.

Another particular feature of the model investigated here is the relatively low level of strangeness featured by the compact stars. As shown in Fig. 3, the  $\Lambda$  states (the first strange particle states to be populated) start to be occupied just before the onset of quark matter, which triggers the unstable branch of compact stars. Thus, the phase transition to quark matter suppresses the presence of strangeness in the object in the local charge neutrality case. Only for the densest objects do we find a small region near the core with a low population of  $\Lambda$  states. The spin down will also affect the strangeness of the object by increasing the radius of strangeness content near the core as the object spins down and becomes denser. This result is shown in Fig. 9 where the relative population ( $\rho_\Lambda/\rho_b$ ) for the  $\Lambda$  states is shown for frequencies of (a) 988.4 Hz, (b) 746.0 Hz, (c) 356.3 Hz, and (d) 0.0 Hz. This result represents the strangeness content of the star, since no other particles that contain strangeness are present. Figure 9 shows that, for higher frequencies (and, thus, for lower densities), strangeness states are either absent or are very lowly populated. As the object spins down and its density increases, the strange core expands and becomes more highly populated. For comparison purposes, in Fig. 10, we

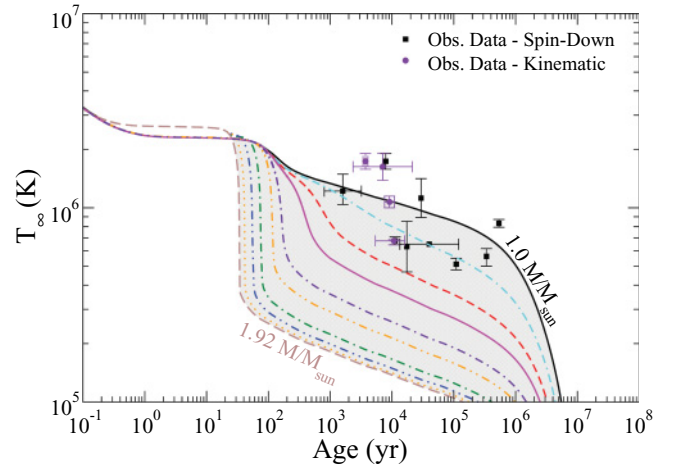


FIG. 11. (Color online) Cooling of a range of spherically symmetric neutron stars from Fig. 2. The symbol  $T_\infty$  denotes the redshifted temperature as detected by an observer at an infinite distance from the star. The onset of the DU process happens for neutron stars with 1.22 solar masses. Any star with a lower mass will have a slow cooling. For masses above this value, an enhanced cooling is achieved. Also shown are some prominently observed temperatures of neutron stars [33,34]. Squares denote that the age was estimated based on the spin-down rate, and circles indicate age estimates based on the motion of the pulsar with respect to its originating supernova remnant.

also show the strangeness content for a  $M_0/M_\odot = 2.38$  star in the pure hadronic model. In this case, since there is no phase transition to quark matter, the stars are able to attain higher masses (as can be seen in Fig. 2). Furthermore, the hyperons are not suppressed by the onset of the quark phase, and these stars attain a higher strangeness content. As shown in Fig. 10, the  $\Lambda$  fraction at the core of the nonrotating star is 3.4 times higher than that found at the core of the densest (stable) hybrid star. Once more, we recall that the different frequencies shown in Figs. 9 and 10 represent different stages of time along the spin evolution of the star, with the time scale that depends on the spin-down rate of the object.

### C. Cooling process

Another method for probing the inner core of compact stars is by investigating its thermal evolution. All the thermal processes, which take place in a compact star, strongly depend on its composition; therefore, by comparing theoretical predictions with observed thermal data, one can obtain valuable information about the cores of neutron stars.

The thermal evolution of neutron stars is dominated by neutrino emissions for the first 1000 years (maybe more in the slow-cooling scenario) [26] and later is replaced by photon emission from the surface. The direct Urca (DU) process [27] is the most efficient cooling mechanism in a neutron star. With emissivities on the order of  $10^{26}$  erg  $\text{cm}^3 \text{s}^{-1}$  [27], neutron stars in which the DU process takes place will cool very quickly. However, because of momentum conservation, the DU process can only take place when the proton fraction reaches a certain value (which depends on the underlying equation of state, but it is usually between 11%–15%). Compact stars, whose proton

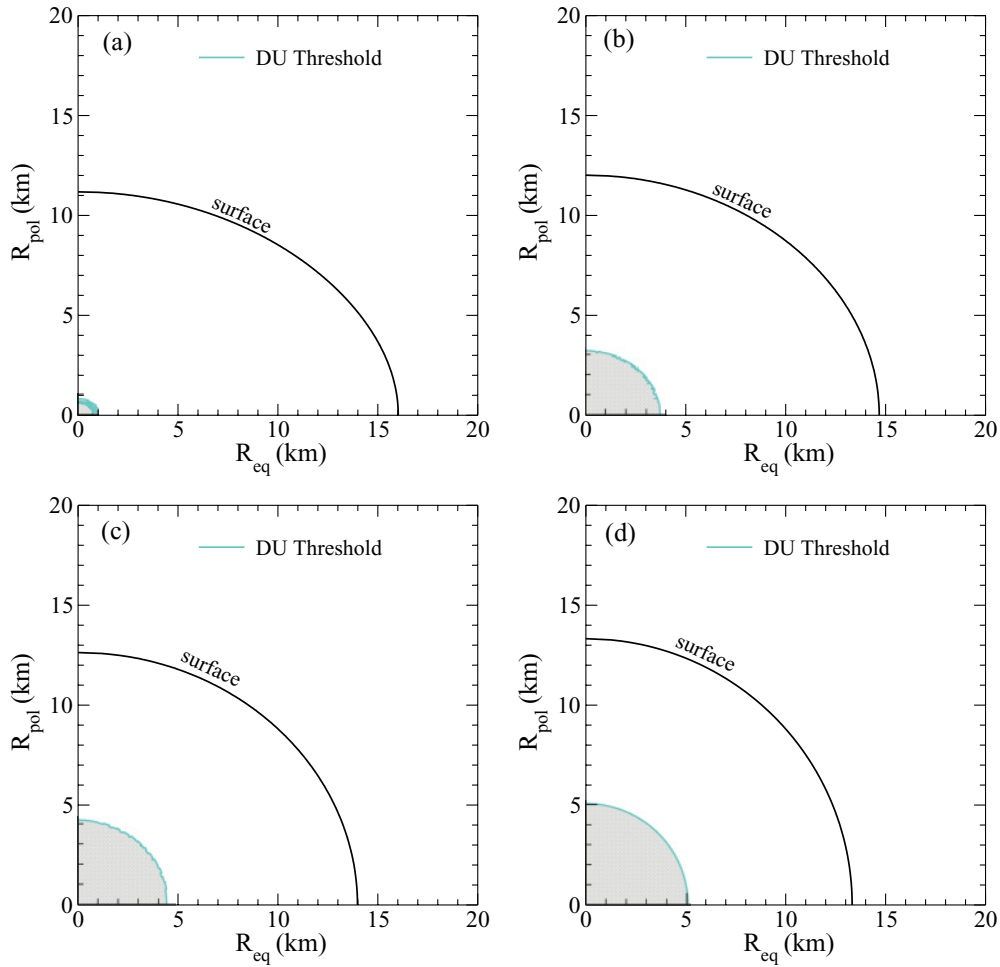


FIG. 12. (Color online) DU threshold for a compact star with  $M_0/M_\odot = 1.6$ , for frequencies of (a) 792.4 Hz, (b) 656.8 Hz, (c) 496.5 Hz, and (d) 0.0 Hz. The gray-shaded areas denote the region in which the DU process is allowed to take place (denoted by  $z = 1$ ).

fractions are below this threshold, will feature a slower cooling. Other processes, such as pairing and meson condensates, for example, might have an influence on whether or not a neutron star will feature a fast or a slow cooling. These topics are beyond the scope of the current research and will be pursued in future investigations.

We solve the thermal evolution equations [28] for the spherically symmetric stars shown in Fig. 2. The emission processes considered for the core are the DU process [27], the modified Urca process [29], and the bremsstrahlung process [29,30]; as for the crust, we consider the electron bremsstrahlung process [31], the electron-positron annihilation [32], and the plasmon decay [32]. The results are shown in Fig. 11 where we show the cooling curves for neutron stars with different gravitational masses. The symbol  $T_\infty$  denotes the redshifted temperature as detected by an observer at an infinite distance from the star.

We have also plotted some prominently observed temperatures of neutron stars [33,34]. Since there are two estimates for the age of pulsars, we have plotted two sets of observed data. The first set is for objects whose age estimate is based on the observed spin-down rate; these are represented by squares. The second set is for ages obtained by tracking the pulsar back

to its original supernova remnant (kinematic age, represented by circles).

As shown in Fig. 11, our model is in relatively good agreement with the observed data, with the exception of a few high-temperature pulsars. It is possible that these objects feature nonstandard processes, such as pairing or some reheating mechanism, which would explain their high temperature. The shaded area represents all possible cooling curves for our model, which can be obtained by solving the cooling equations for the whole spectrum of stable hybrid stars shown in Fig. 2. We can also see that, within our model, neutron stars with masses higher than 1.22 solar masses, which feature an enhanced cooling, cool down too fast to be in agreement with observed data. It is important to mention that these results can be further improved if one considers more sophisticated processes, such as pairing and meson condensation.

Finally, we have also investigated how spin-down effects might affect the thermal evolution. As shown in Fig. 9, the increase in density that follows spin down has a strong effect on the strangeness content of the star. It is only natural to expect that other particle states will also be altered by the spin down. Particularly interesting is the proton, electron, and neutron populations, since these particle populations will

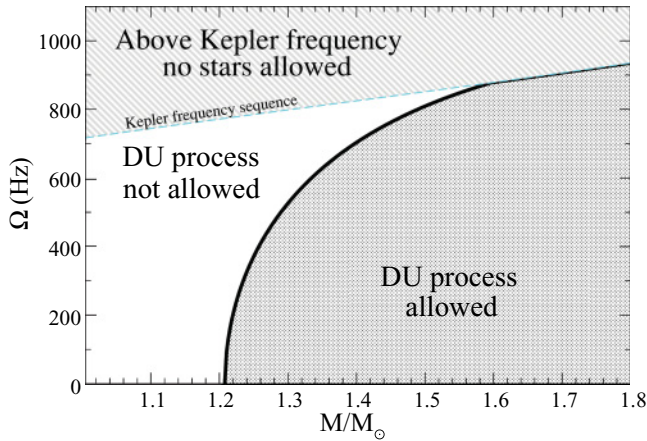


FIG. 13. (Color online)  $\Omega(M)$  diagram. Any star with mass and frequency that falls within the dark-gray-shaded area allows for the DU process to take place. The light-gray-shaded area, on the top of the diagram, represents a forbidden region, where no stars can be found, since their frequencies would be above their Kepler frequencies. Finally, the white area represents stars in which the DU process cannot take place.

dictate whether or not the DU process will take place. This process can only take place if the following triangle inequality (and cyclic permutations of it) are satisfied

$$k_n^f + k_p^f \geq k_e^f, \quad (8)$$

with  $k_i^f$  as the Fermi momentum of particle  $i$ . We calculated the radius threshold for different frequency stars from the sequence with  $M_0/M_\odot = 1.6$ . This result is shown in Fig. 12, where the gray-shaded areas represent the region in which the DU process is allowed to take place.

The results of Fig. 12 show that the region in which the DU process takes place changes substantially during the evolution of the compact star. For the case studied, for higher frequencies (where the density is lower), the DU process can only take place in a very small region near the core. This region grows as the stellar frequency decreases and the object becomes denser. This hints that the cooling of compact stars might be slower if one considers effects of spin down. Current efforts are in progress to better understand this issue and will be discussed in a future paper.

Finally, we also have generated a diagram  $\Omega(M)$  that shows the domain of frequencies and mass for which the DU process is allowed. This result is shown in Fig. 13, where any star with mass and frequency that falls within the dark-gray-shaded area allows for the DU process to take place. The light-gray-shaded area, on the top of the diagram, represents a forbidden region, where no stars can be found, since their frequencies would be above their Kepler frequencies. The white area represents stars in which the DU process cannot take place. Currently, the spin of many x-ray burst sources is known, and in some cases, their masses can also be inferred (see Refs. [35–37] and references therein). In the case of transient neutron stars, the core temperature can be inferred from the quiescent emission state [38]. Furthermore, for some neutron stars, the spin frequency and the core temperature are bound (see, for

instance, Ref. [39]). In the event that one might estimate the core temperature, the spin frequency, and the stellar mass, the diagram shown in Fig. 13 might be used as a further test for this model.

#### IV. CONCLUSION

A major advantage of our paper, when compared to other studies of hybrid stars, is that, because we have only one equation of state for different degrees of freedom, we can study, in detail, the way in which chiral symmetry is restored and the way deconfinement occurs in the stars. Such phenomena happen, for example, during the star spin down.

We have found that the SU(3) nonlinear  $\sigma$  model is suitable for the description of hybrid stars. The predicted maximum masses and the respective radii lie in the observed range. For a static object, our model predicts a star that contains 2 km of hybrid matter (radius) surrounded by hadronic matter. In the event that the object is rotating at its Kepler frequency, the hybrid core becomes an oblate ellipsoid with equatorial and polar radii of 1.18 and 0.87 km, respectively. The reduction of the quark core for a rotating object should not be surprising if one considers the reduction in density that follows rapid rotation.

Also, we have investigated the cooling of spherically symmetric (static) neutron stars, whose composition is described by our model. We have found that the threshold for the DU process is reached for stars with masses greater than  $1.0 M_\odot$ . We have compared the cooling curves predicted by our model with some prominently observed compact star temperatures. We have found that, within our model, objects with masses up to  $1.22 M_\odot$  are in good agreement with the observed data. Any star with a mass above this value features a thermal evolution that is too fast to be in agreement with the observed data. This result might seem inconsistent with the observed data, since most of these objects are expected to have a mass higher than  $1.22 M_\odot$ . It is important to notice that the results shown in Fig. 11 were obtained by assuming a froze-in structure/composition. As noted in Ref. [38], many observed accreting neutron stars are in agreement with the slow-cooling scenario. The fact that they are accreting implies that their structures are changing, as their frequencies are modified as a result of the accretion process. As we showed in Fig. 12, the threshold radius for the DU process strongly depends on the frequency of the star. Therefore, the fast cooling for stars with masses above  $1.22 M_\odot$  might be deceiving, since, if we consider rotation, we might obtain stars with  $M_0 = 1.6 M_\odot$  without presenting the DU process (if the frequency is high enough). We could also see that a few observed objects present a very high temperature, which cannot be explained by our model. Most likely, there is some nontrivial heating process that takes place in these objects, which would explain why they are so warm at their relatively old ages; this topic, however, is beyond the scope of this paper. It is important to mention that the quarks found in the 2-km hybrid core have little effect on the cooling of these objects. Not only is the hybrid core very small, but also the quarks are present at a smaller ratio than the hadrons, which allows the hadrons to dominate the cooling processes. On the other hand, the suppression of hyperons caused by the onset of the quark phase is important. Since

the hyperons do not appear in great quantities, some cooling channels (hyperon Urca processes, for instance) are not open. These channels are not very efficient cooling mechanisms [40], nonetheless, their absence slows down the cooling.

#### ACKNOWLEDGMENT

We acknowledge access to the computing facility of the Center of Scientific Computing at the Goethe-University Frankfurt for our numerical calculations.

- 
- [1] H. Heiselberg, C. J. Pethick, and E. F. Staubo, *Phys. Rev. Lett.* **70**, 1355 (1993).
- [2] K. Fukushima, *Phys. Lett. B* **591**, 277 (2004).
- [3] V. A. Dexheimer and S. Schramm, *Phys. Rev. C* **81**, 045201 (2010).
- [4] P. Papazoglou, S. Schramm, J. Schaffner-Bielich, H. Stöcker, and W. Greiner, *Phys. Rev. C* **57**, 2576 (1998).
- [5] P. Papazoglou, D. Zschesche, S. Schramm, J. Schaffner-Bielich, H. Stöcker, and W. Greiner, *Phys. Rev. C* **59**, 411 (1999).
- [6] V. Dexheimer and S. Schramm, *Astrophys. J.* **683**, 943 (2008).
- [7] C. Ratti, M. Thaler, and W. Weise, *Phys. Rev. D* **73**, 014019 (2006).
- [8] S. Rößner, C. Ratti, and W. Weise, *Phys. Rev. D* **75**, 034007 (2007).
- [9] R. Tolman, *Phys. Rev.* **55**, 364 (1939).
- [10] J. Oppenheimer and G. Volkoff, *Phys. Rev.* **55**, 374 (1939).
- [11] R. N. Manchester, G. B. Hobbs, A. Teoh, and M. Hobbs, *Astron. J.* **129**, 1993 (2005).
- [12] I. H. Stairs, *Science* **304**, 547 (2004).
- [13] J. Latimmer and M. Prakash, *Phys. Rep.* **442**, 109 (2007).
- [14] J. P. W. Verbiest, M. Bailes, W. van Straten, G. B. Hobbs, R. T. Edwards, R. N. Manchester, N. D. R. Bhat, J. M. Sarkissian, B. A. Jacoby, and S. R. Kulkarni, *Astrophys. J.* **679**, 675 (2008).
- [15] P. C. C. Freire, A. Wolszczan, M. van Den Berg, and J. W. T. Hessels, *Astrophys. J.* **679**, 1433 (2008).
- [16] D. J. Champion *et al.*, *Science* **320**, 1309 (2008).
- [17] A. Kurkela, P. Romatschke, A. Vuorinen, and B. Wu, *Phys. Rev. D* **81**, 105021 (2010).
- [18] G. Baym, C. Pethick, and P. Sutherland, *Astrophys. J.* **170**, 299 (1971).
- [19] N. K. Glendenning, *Phys. Rev. D* **46**, 1274 (1992).
- [20] V. Dexheimer and S. Schramm, *Phys. Rev. C*, **81**, 045201 (2010).
- [21] S. Schramm and D. Zschesche, *J. Phys. G* **29**, 531 (2003).
- [22] N. K. Glendenning and F. Weber, *Phys. Rev. D* **50**, 3836 (1994).
- [23] H. Komatsu, Y. Eriguchi, and I. Hachisu, *R. Astron. Soc., Monthly Notices* **237**, 355 (1989).
- [24] G. B. Cook, S. L. Shapiro, and S. A. Teukolsky, *Astrophys. J.* **398**, 203 (1992).
- [25] N. Stergioulas and J. L. Friedman, *Astrophys. J.* **444**, 306 (1995).
- [26] D. Page, U. Geppert, and F. Weber, *Nucl. Phys. A* **777**, 497 (2006).
- [27] J. Lattimer, C. Pethick, M. Prakash, and P. Haensel, *Phys. Rev. Lett.* **66**, 2701 (1991).
- [28] F. Weber, *Pulsars as Astrophysical Laboratories for Nuclear and Particle Physics*, 1st ed. (Institute of Physics, Bristol, UK, 1999).
- [29] B. L. Friman and O. V. Maxwell, *Astrophys. J.* **232**, 541 (1979).
- [30] O. V. Maxwell, *Astrophys. J.* **231**, 201 (1979).
- [31] A. D. Kaminker, C. J. Pethick, A. Y. Potekhin, V. Thorsson, and D. G. Yakovlev, *Astron. Astrophys.* **343**, 1009 (1999).
- [32] D. Yakovlev, *Phys. Rep.* **354**, 1 (2001).
- [33] D. Page, J. M. Lattimer, M. Prakash, and A. W. Steiner, *Astrophys. J. Suppl. Ser.* **155**, 623 (2004).
- [34] D. Page, J. M. Lattimer, M. Prakash, and A. W. Steiner, *Astrophys. J.* **707**, 1131 (2009).
- [35] F. Ozel, *Nature (London)* **441**, 1115 (2006).
- [36] A. W. Steiner, J. M. Lattimer, and E. F. Brown [arXiv:1005.0811](https://arxiv.org/abs/1005.0811) [astro-ph.HE].
- [37] V. Suleimanov, J. Poutanen, M. Revnivtsev, and K. Werner [arXiv:1004.4871](https://arxiv.org/abs/1004.4871) [astro-ph.HE].
- [38] C. O. Heinke, P. G. Jonker, R. Wijnands, and R. E. Taam, *Astrophys. J.* **660**, 1424 (2007).
- [39] E. F. Brown, L. Bildsten, and P. Chang, *Astrophys. J.* **574**, 920 (2002).
- [40] M. Prakash, J. Lattimer, and C. Pethick, *Astrophys. J.* **390**, L77 (1992).